

Cyclin B1 acts as a tumor microenvironment-related cancer promoter and prognostic biomarker in hepatocellular carcinoma

Journal of International Medical Research
49(5) 1–19

© The Author(s) 2021

Article reuse guidelines:

sagepub.com/journals-permissions

DOI: 10.1177/03000605211016265

journals.sagepub.com/home/imr



Yangming Hou, Xin Wang, Junwei Wang,
Xuemei Sun, Xinbo Liu , Han Hu,
Wenzhe Fan, Xinchun Zhang and Dequan Wu 

Abstract

Objectives: The present study aimed to develop a gene signature based on the ESTIMATE algorithm in hepatocellular carcinoma (HCC) and explore possible cancer promoters.

Methods: The ESTIMATE and CIBERSORT algorithms were applied to calculate the immune/stromal scores and the proportion of tumor-infiltrating immune cells (TICs) in a cohort of HCC patients. The differentially expressed genes (DEGs) were screened by Cox proportional hazards regression analysis and protein–protein interaction (PPI) network construction. Cyclin B1 (CCNB1) function was verified using experiments.

Results: The stromal and immune scores were associated with clinicopathological factors and recurrence-free survival (RFS) in HCC patients. In total, 546 DEGs were up-regulated in low score groups, 127 of which were associated with RFS. CCNB1 was regarded as the most predictive factor closely related to prognosis of HCC and could be a cancer promoter. Gene Set Enrichment Analysis (GSEA) and CIBERSORT analyses indicated that CCNB1 levels influenced HCC tumor microenvironment (TME) immune activity.

Conclusions: The ESTIMATE signature can be used as a prognosis tool in HCC. CCNB1 is a tumor promoter and contributes to TME status conversion.

Department of Hepatic Surgery, The Second Affiliated Hospital of Harbin Medical University, Harbin, Heilongjiang, China

Corresponding author:

Dequan Wu, Department of Hepatic Surgery, The Second Affiliated Hospital of Harbin Medical University, No. 246 Xuefu Avenue, Harbin, Heilongjiang 150086, China.
Email: dquwu58@163.com



Creative Commons Non Commercial CC BY-NC: This article is distributed under the terms of the Creative Commons Attribution-NonCommercial 4.0 License (<https://creativecommons.org/licenses/by-nc/4.0/>) which permits non-commercial use, reproduction and distribution of the work without further permission provided the original work is attributed as specified on the SAGE and Open Access pages (<https://us.sagepub.com/en-us/nam/open-access-at-sage>).

Keywords

Hepatocellular carcinoma, tumor microenvironment, recurrence, *CCNB1*, prognostic biomarker, survival

Date received: 25 August 2020; accepted: 19 April 2021

Introduction

Based on the latest global cancer epidemic statistics (GLOBOCAN), hepatocellular carcinoma (HCC) is one of the most fatal diseases, ranking fourth among all tumors worldwide.¹ HCC accounts for 70% to 85% of primary liver cancers with about 750,000 new cases and 700,000 deaths each year.¹ HCC patients are frequently diagnosed at advanced stage with 5-year survival rates less than 30%.² At present, treatment for HCC mainly includes surgical resection, interventional therapy, and percutaneous ablation. Chemotherapy and targeted therapies are generally less effective. It is therefore necessary to identify more effective molecular biomarkers and therapeutic targets. To achieve this goal, researchers have established certain whole gene expression data sets, including The Cancer Genome Atlas (TCGA) database, to analyze genomic abnormalities in cancer cases.³

Intrinsic genes, especially main transcription factors, have always been the focus of malignancy research. However, it has been suggested that the tumor microenvironment (TME) is of critical importance for tumor-associated gene expression.⁴ The TME is the cellular milieu around where the tumor is located. It is considered to be a crucial factor for determining the survival and proliferation of tumor cells in metastatic lesions.⁵ In addition to tumor cells, the TME of HCC is composed of stromal cells, extracellular matrix, and intercellular communication molecules that regulate immune

escape and immune therapy response of HCC cells.⁶ To assess the tumor purity of the TME, Yoshihara et al.⁴ established a computational method called Estimation of STromal and Immune cells in Malignant Tumor tissues using Expression data (ESTIMATE). By analyzing gene expression characteristics, the algorithm can calculate immune and stromal scores as main parameters. In subsequent studies, the ESTIMATE program was applied to prostate cancer,⁷ breast cancer,⁸ colon cancer,⁹ and glioblastoma,¹⁰ demonstrating the effectiveness of this big data-based algorithm. However, the usefulness of the ESTIMATE algorithm in HCC has not been investigated in detail.

CCNB1, the gene coding for cyclin B1, belongs to the highly conserved cyclin family and is a regulatory factor involved in mitosis and cell cycle progression.¹¹ It is broadly expressed in lymph node tissue and provides proper control for the G2/M phase transition. In addition, *CCNB1* combines with p34(*cdc2*) to form the maturation-promoting factor (MPF).¹² Here, by further comparing differentially expressed genes (DEGs), we demonstrate that *CCNB1* is a potential factor responsible for the change of TME status in HCC.

Materials and methods

Ethical approval

The data used in this study were from TCGA database; consent and ethics-related

documents can be found here: <https://www.cancer.gov/about-nci/organization/ccg/research/structural-genomics/tcga/history/policies>. Further ethical approval was given by Second Affiliated Hospital of Harbin Medical University.

TCGA Data

Gene expression profiles of HCC tumors were accessed from the TCGA database (<https://tcga-data.nci.nih.gov/tcga/>), which was measured experimentally using the Illumina HiSeq 2000 RNA Sequencing platform by the University of North Carolina TCGA genome characterization center.³ This dataset shows gene-level transcriptional estimates, as in $\log_2(x+1)$ transformed RSEM normalized count. Clinical data were also obtained from the same portal. Immune scores and stromal scores were gained by running ESTIMATE computational methods.⁴ For results verification, a gene expression profile GSE54236 was downloaded from the Gene Expression Omnibus (GEO) database (GPL6480 platform, GPL6480 Agilent-014850 Whole Human Genome Microarray 4x44K G4112F). According to the platform annotation information, the probes were transformed into the corresponding genetic symbol.

Identification of differentially expressed genes (DEGs)

Overall, 232 HCC cases were divided into upper and lower halves relative to the median values of the immune and stromal scores. The limma package was used to perform data analysis.¹³ The cut-off value was set as fold change > 1.5 and adj. $P < 0.05$ to filter the TCGA data and identify DEGs, which were generated by the comparison between the high-score cases vs. the low-score cases.

Heatmaps

The open-source web tool ClustVis was used to build heatmaps.¹⁴

Protein–protein interaction (PPI) network construction

Data for protein–protein interaction (PPI) networks were provided by the Search Tool for the Retrieval of Interacting Genes (STRING; <http://string-db.org>) (version 10.0)¹⁵ and constructed by Cytoscape software.¹⁶ The topological clustering tool Molecular Complex Detection (MCODE) (version 1.4.2) was used to detect densely connected clusters.¹⁷

Enrichment analysis of DEGs

Gene Ontology (GO) and Kyoto Encyclopedia of Genes and Genomes (KEGG) enrichment analyses were performed with the cluster Profiler, enrichplot, and ggplot2 packages. The items with $P < 0.05$ were considered significantly enriched.

Enrichment analysis of gene sets

Gene Set Enrichment Analysis (GSEA)-3.0 software was used to perform the analysis. Hallmark, KEGG, GO, and C7 gene sets of v6.2 collections were obtained as the target set from the Molecular Signatures Database. Listed gene sets with nominal (NOM) $P < 0.05$ were considered statistically significant.

Tumor-infiltrating immune cell (TIC) profiles

The distribution of tumor-infiltrating immune cells (TICs) abundance in all tumor samples was estimated using the CIBERSORT calculation method. The cases with $P < 0.05$ were filtered for further analysis.

Tissue collection

Paraffin-embedded HCC specimens and paired non-cancerous tissues from 108 patients were selected from the Department of General Surgery, Second Affiliated Hospital of Harbin Medical University (Harbin, China) between January 2013 and January 2015. The study protocol was approved by the Ethics Committee of the Second Affiliated Hospital of Harbin Medical University and samples were obtained with written informed consent.

Immunohistochemical staining analysis

In brief, 4- μ m-thick sections were cut from paraffin-embedded specimens, then deparaffinized, rehydrated, and heated according to procedural standards. Subsequently, the sections were placed in 3% hydrogen peroxide at room temperature for 10 minutes to remove endogenous peroxidase activity, followed by blocking with 1% bovine serum albumin (BSA). The samples were then incubated with a CCNB1 primary antibody (1:100 ABclonal, Wuhan, China) at 4°C overnight. Finally, the sections were incubated with biotin-labeled secondary antibody (1:100; HY90046; Shanghai HengYuan Biological Technology Co. Ltd., Shanghai, China) at 37°C for 30 minutes and horse-radish peroxidase-conjugated streptavidin for 20 minutes. A Leica DM4000B/M microscope (Leica Microsystems, Inc., Buffalo Grove, IL, USA) was used for observation.

Cell culture and transfections

Huh7 and HepG2 cells were obtained from the American Type Culture Collection (ATCC). Both cell lines were cultured in Dulbecco's modified Eagle's medium (DMEM) supplemented with 10% fetal bovine serum (FBS) (Thermo Fisher Scientific, Waltham, MA, USA) and

incubated at 37°C and 5% CO₂. A small interfering RNA (siRNA) against CCNB1 and scrambled siRNA negative control were synthesized by GenePharma (Shanghai, China). Transient transfections in cells were performed with Lipofectamine 2000 (Thermo Fisher Scientific) according to the manufacturer's instructions.

Immunofluorescence assay

Cells were seeded in culture dishes and grown for 2 days. Cells in the logarithmic phase of growth were washed with phosphate buffered saline (PBS) and fixed with 4% paraformaldehyde at room temperature for 30 minutes. A 0.2% Triton X-100 solution was used to permeabilize cell membranes. After blocking in 5% BSA for 30 minutes, the cells were incubated with a CCNB1 primary antibody (1:100 ABclonal) at 4°C overnight. The cells were further washed with PBS three times and incubated with fluorescence-conjugated secondary antibodies for 1 hour. The nuclei were stained with 4',6-Diamidino-2'-phenylindole dihydrochloride (DAPI, C1002, Beyotime, Shanghai, China). Finally, immunofluorescence images were captured by confocal microscope (Olympus FV1000, Japan).

Cell proliferation, migration, and invasion assays

Cell Counting Kit (CCK)-8 assays (C0038, Beyotime) were used to evaluate the proliferation rates of untreated and CCNB1-deficient HCC cells. 2×10^3 cells were plated in 96-well plates and the absorbance readings at 450 nm were recorded every 24 hours. For Transwell migration and Matrigel invasion assays, cells were incubated for 24 hours, then any migrated cells were fixed with methanol and stained with crystal violet. Cell migration and invasion were observed under a microscope.

Establishment of animal models

Animal models were established based on institutional protocols and approved by the Animal Ethics Committee of Harbin Medical University. For *in vivo* experiments, 4-week-old male BALB/c nude mice were injected with equal numbers of HCC cells stably infected with pL/shRNA/F-CCNB1 or pL/shRNA/F (5×10^6 cells/injection for Huh7 cells). These vectors are for a short hairpin RNA (shRNA) against CCNB1 and control shRNA. About 4 weeks after xenotransplantation, mice were sacrificed and xenografts were removed, weighed, and photographed. Tumor diameters were observed with a precision caliper to calculate the mass volume.

Statistical analysis and survival curves

SPSS 20.0 software (IBM, Armonk, NY, USA) and GraphPad Prism 7.0 (GraphPad Software, San Diego, CA, USA) were used for statistical analysis. All results are expressed as mean \pm standard deviation (SD). Data for non-parametric variables were evaluated by chi-square tests. Student's t-tests were used for parametric variables. The relationships between DEG expression levels and patient recurrence-free survival (RFS) were illustrated with Kaplan–Meier plots and Cox proportional hazards regression models. The results were tested using log-rank tests. P -values < 0.05 were regarded as statistically significant.

Results

Immune and stromal scores are significantly correlated with clinicopathological factors and RFS of HCC patients

We screened data from TCGA database for HCC cases that received only radical

resection with RFS more than 30 days. Ultimately, 232 cases were enrolled. The ESTIMATE method was used to obtain immune and stromal scores and then analyze both with clinicopathological factors. Statistics indicated that the stromal score was associated with histological grade ($P=0.006$), body mass index (BMI) ($P=0.018$), and hepatitis virus infection ($P=0.025$). The immune score was relevant with the clinical stage ($P=0.007$), but the stromal score ($P=0.070$) was not statistically significant (Table 1).

To demonstrate the potential relationship between RFS and immune and/or stromal scores, 232 HCC cases were divided into upper and lower halves (high vs. low groups). According to the Kaplan–Meier survival curves (Table 2), the median RFS of the high stromal score group was longer than that of the low score group (1432 days vs. 776 days, $P=0.0326$). Consistently, the high immune score group also had longer median RFS than the low score group (2028 days vs. 592 days, $P < 0.0001$). In addition, we performed prognostic statistical analysis of other pathological factors and confirmed that clinical stage ($P < 0.001$), microvascular invasion (MVI) ($P=0.026$), surgical method ($P < 0.001$), and viral hepatitis ($P=0.008$) were also associated with RFS (Table 2).

Parameters confirmed as significant in the univariate log-rank test, along with some important clinicopathological factors, were included in the multivariate Cox regression model. The statistics indicated that the immune score ($P=0.003$, Table 3) could possibly serve as an independent prognostic marker for RFS. Furthermore, clinical stage ($P=0.005$), BMI ($P=0.038$), and surgical method ($P=0.027$) were also significantly associated with prognosis. The stromal score ($P=0.238$) also showed a trend of relevance, although it was not statistically significant (Table 3).

Table 1. Association between immune and/or stromal scores and clinicopathological characteristics in hepatocellular carcinoma (HCC) patients.

Variable	Number of Patients	Immune scores		Stromal scores	
		Mean \pm SE	P-value	Mean \pm SE	P-value
Age, years			0.588		0.197
≤ 50	44	23.36 \pm 119.3		-637.8 \pm 98.22	
> 50	188	-37.85 \pm 46.91		-760.7 \pm 39.84	
Sex			0.755		0.215
Female	78	-6.839 \pm 83.36		-672.2 \pm 68.43	
Male	154	-36.07 \pm 51.56		-770.4 \pm 44.17	
Histological grade			0.936		0.006
G1/G2	144	-28.02 \pm 52.69		-660.5 \pm 46.53	
G3/G4	85	-20.57 \pm 81.27		-872.5 \pm 61.16	
Clinical stage			0.007		0.070
I/II	164	46.59 \pm 53.15		-713.7 \pm 44.66	
III/IV	55	-240.2 \pm 86.2		-873.1 \pm 71.79	
Child-Pugh			0.325		0.347
A	145	-31.66 \pm 52.51		-774.3 \pm 44.12	
B	11	-223.5 \pm 131.8		-926.8 \pm 67.58	
MVI			0.858		0.504
No	131	-10.53 \pm 54.29		-693.3 \pm 47.99	
Yes	68	-27.98 \pm 86.18		-748.8 \pm 68.31	
BMI			0.127		0.018
> 30	39	131 \pm 93.79		-541.1 \pm 88.9	
≤ 30	178	-53.29 \pm 52.32		-781.1 \pm 42.79	
Surgical method			0.198		0.678
Segmentectomy	110	33.65 \pm 58.15		-721 \pm 49.71	
Lobectomy or more extensive	122	-80.25 \pm 65.39		-752.2 \pm 55.17	
Viral hepatitis			0.362		0.025
No	125	-67.49 \pm 60.97		-657 \pm 55.62	
Yes	98	13.13 \pm 62.34		-828.9 \pm 48.68	

SE, standard error; MVI, microvascular invasion; BMI, body mass index.

Identification of DEGs with stromal and/or immune scores in HCC

We compared RNA-sequencing (RNA-seq) data of low vs. high immune/stromal scores cohorts (Figure 1a,b) and identified 433 and 174 up-regulated genes in the low stromal and low immune score groups, respectively (fold change > 1.5 , $P < 0.05$). A total of 546 genes were up-regulated in both groups, of which 61 genes were commonly up-regulated (Figure 1c). Therefore, we decided to

focus on all of these up-regulated DEGs for follow-up analysis. The most significant features of GO enrichment analysis are shown in Figure 1d, including nuclear division, chromosome segregation, and organelle fission. By KEGG enrichment analysis, up-regulated DEGs were enriched in cell cycle and metabolism of xenobiotics by cytochrome P450 signaling pathways (Figure 1e). Therefore, the overall function of these DEGs seems to be related to tumor development.

Table 2. Univariate survival analysis of recurrence-free survival (RFS) in hepatocellular carcinoma (HCC) patients.

Variable	Number of Patients	RFS, days		P-value
		Mean \pm SE	95% CI	
Age, years	232			0.672
≤ 50	44	1818.316 \pm 285.357	1259.016–2377.615	
> 50	188	1669.700 \pm 153.615	1368.615–1970.785	
Sex	232			0.720
Female	78	1615.500 \pm 217.732	1188.746–2042.254	
Male	144	1789.001 \pm 182.831	1430.653–2147.350	
Histological grade	229			0.817
G1/G2	144	1765.843 \pm 185.521	1402.222–2129.465	
G3/G4	85	1689.040 \pm 217.697	1262.354–2115.727	
Clinical stage	219			<0.001
I/II	164	1956.825 \pm 163.468	1636.429–2277.222	
III/IV	55	1063.767 \pm 219.376	633.790–1493.743	
Child–Pugh	156			0.388
A	145	1912.731 \pm 162.432	1594.363–2231.098	
B	11	886.494 \pm 180.279	533.146–1239.841	
MVI	199			0.026
No	131	1998.034 \pm 189.834	1625.959–2370.108	
Yes	68	1446.866 \pm 214.193	1027.048–1866.683	
BMI	217			0.528
> 30	39	1536.500 \pm 208.968	1126.924–1946.076	
≤ 30	178	1834.925 \pm 169.957	1501.809–2168.041	
Surgical method	232			<0.001
Segmentectomy	110	2122.755 \pm 203.707	1723.490–2522.020	
Lobectomy or more extensive	122	1315.669 \pm 176.555	969.622–1661.716	
Viral hepatitis	223			0.008
No	125	1480.526 \pm 178.412	1130.838–1830.213	
Yes	98	2110.592 \pm 230.409	1658.990–2562.194	
Stromal score	232			0.033
Low	116	1732.036 \pm 167.664	1403.414–2060.658	
High	116	1585.302 \pm 220.290	1153.534–2017.070	
Immune score	232			<0.001
Low	116	2170.100 \pm 199.015	1780.031–2560.170	
High	116	993.541 \pm 109.341	779.231–1207.850	

RFS, recurrence-free survival; SE, standard error; CI, confidence interval; MVI, microvascular invasion; BMI, body mass index.

Correlation between individual DEG expression and RFS with univariate Cox regression

To further screen the DEGs related to RFS, a Cox proportional hazards regression

model was generated. Among the 546 up-regulated genes, 127 were shown to be significantly associated with poor prognosis ($P < 0.05$) (Appendix).

We replicated the analysis in microarray dataset GSE54236 of 81 HCC cases from

Table 3. Multivariate Cox regression analysis for various potential prognostic characteristics of recurrence-free survival (RFS) in hepatocellular carcinoma (HCC) cases.

Variable	RFS		
	Exp(B)	95% CI	P-value
Histological grade	1.543	0.844–2.820	1.543
Clinical stage	2.419	1.299–4.505	0.005
Child–Pugh	1.438	0.520–3.976	0.484
MVI	0.915	0.465–1.799	0.796
BMI	0.489	0.249–0.961	0.038
Surgical method	1.957	1.080–3.545	0.027
Viral hepatitis	1.072	0.559–2.058	0.834
Immune scores	2.586	1.378–4.852	0.003
Stromal scores	1.469	0.776–2.781	0.238

RFS, recurrence-free survival; CI, confidence interval; MVI, microvascular invasion; BMI, body mass index.

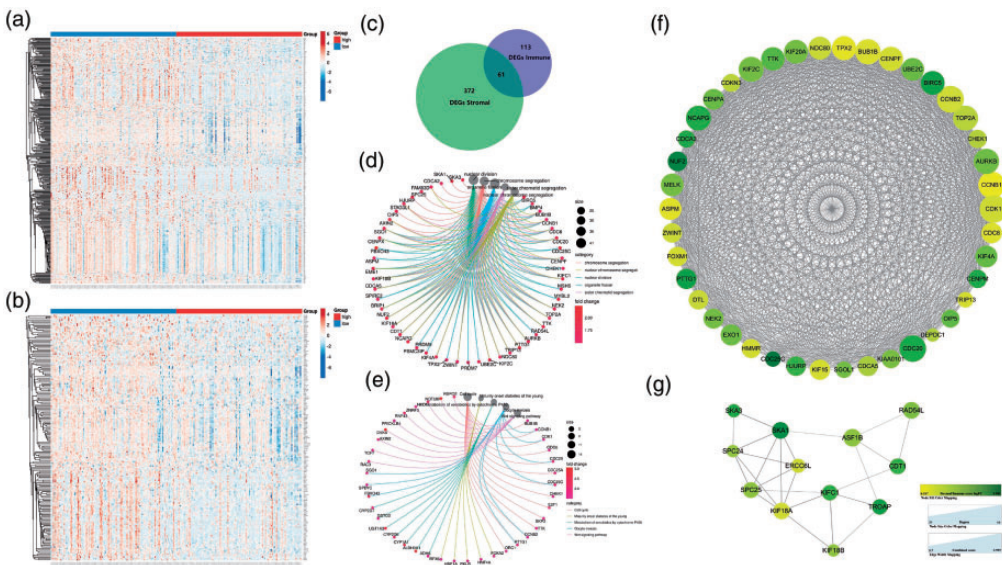


Figure 1. Differential gene expression profiles with stromal/immune scores and protein–protein interaction (PPI) networks in HCC cases. (a) Heatmap of the differentially expressed genes (DEGs) in the low vs. high immune score groups. (Fold change > 1.5, $P < 0.05$). (b) Heatmap of the DEGs in the low vs. high stromal score groups. (Fold change > 1.5, $P < 0.05$). (c) Venn diagrams of upregulated DEGs in both the stromal and immune score groups. (d) Gene Ontology (GO) enrichment analysis of 546 DEGs (The cutoff value was set as P and $q < 0.05$). (e) Kyoto Encyclopedia of Genes and Genomes (KEGG) enrichment analysis of 546 DEGs (P and $q < 0.05$). (f) Protein–protein interaction (PPI) networks of the cyclin-dependent kinase I (CDKI) module. (g) PPI networks of the anti-silencing function IB histone chaperone (ASF1B) module. The heatmaps were constructed by ClustVis. The enrichment analyses were produced by R language with the packages of enrichplot. The PPI networks were constructed using Cytoscape. The size of nodes reflects the number of interacting proteins with the designated ones. The edge width indicates the combined scores obtained from STRING.

the GEO database.¹⁸ A total of 117 DEGs could be obtained from the dataset. By establishing the Cox proportional hazards regression model, 93 DEGs were confirmed to be significantly related to survival time and 98 were significantly correlated with tumor doubling time. After summarizing the above data, 103 genes were found to be involved in both groups, and the two groups almost completely coincided. The above results further suggest the accuracy of the DEG screening.

PPI network construction among genes with preliminary prognostic value and module analysis with multivariate Cox regression

To better illustrate the interaction among RFS-related DEGs, we constructed PPI networks with STRING and Cytoscape (Figure 1f,g). After excluding the isolated nodes, a network of DEGs was established composed of two modules, including 80 nodes and 1343 edges. Both modules were selected for further analysis and named as CDK1 and ASF1B. The CDK1 module (Figure 1f) was formed by 796 edges and 42 nodes, among which all factors had identical MCODE scores of more than 25 points. CDK1, CCNB2, CCNB1, and CDC20 were defined as the remarkable nodes, for they had the highest relevance degree. In the ASF1B module (Figure 1g), 12 DEGs were included.

The nodes in both modules were added to the multivariate Cox regression model together with significant clinical pathological factors including BMI, MVI, surgical method, tumor grade, and stage. Statistical results suggested that CCNB1, DNA topoisomerase II alpha (TOP2A), ubiquitin conjugating enzyme E2 (UBE2C), and ZW10 interacting kinetochore protein (ZWINT) could be used as independent prognostic genes of RFS in

Table 4. Multivariate Cox regression analysis for various potential differentially expressed genes (DEGs) and prognostic characteristics of recurrence-free survival (RFS) in hepatocellular carcinoma (HCC) cases.

Variable	RFS		
	Exp(B)	95% CI	P-value
Module 1			
Stage	3.205	1.830–5.613	<0.001
TOP2A	1.818	1.119–2.954	0.016
UBE2C	1.734	1.047–2.874	0.033
CCNB1	1.745	1.011–3.010	0.046
ZWINT	2.759	1.534–4.961	0.001
Module 2			
Stage	2.981	1.750–5.079	<0.001
ERCC6L	1.211	1.008–1.456	0.041

RFS, recurrence-free survival; CI, confidence interval; TOP2A, DNA topoisomerase II alpha; UBE2C, ubiquitin conjugating enzyme E2; CCNB1, cyclin B1; ZWINT, ZW10 interacting kinetochore protein; ERCC6L, ERCC excision repair 6 like, spindle assembly checkpoint helicase.

the CDK1 module (Table 4). In the ASF1B module, only ERCC excision repair 6 like, spindle assembly checkpoint helicase (ERCC6L) was regarded as an independent prognostic factor.

Correlation of CCNB1 expression with survival and clinicopathological factors of HCC patients

Because our findings revealed that CCNB1 had the highest degree of relevance, we moved forward with this gene as our research focus. All HCC samples were divided into high and low expression groups according to the median expression level of CCNB1. Wilcoxon rank sum tests indicated that CCNB1 expression was significantly higher in HCC tumor samples than in normal tissues (Figure 2a). An accordant result was obtained in paired analysis (Figure 2b). Survival analysis revealed that RFS and overall survival

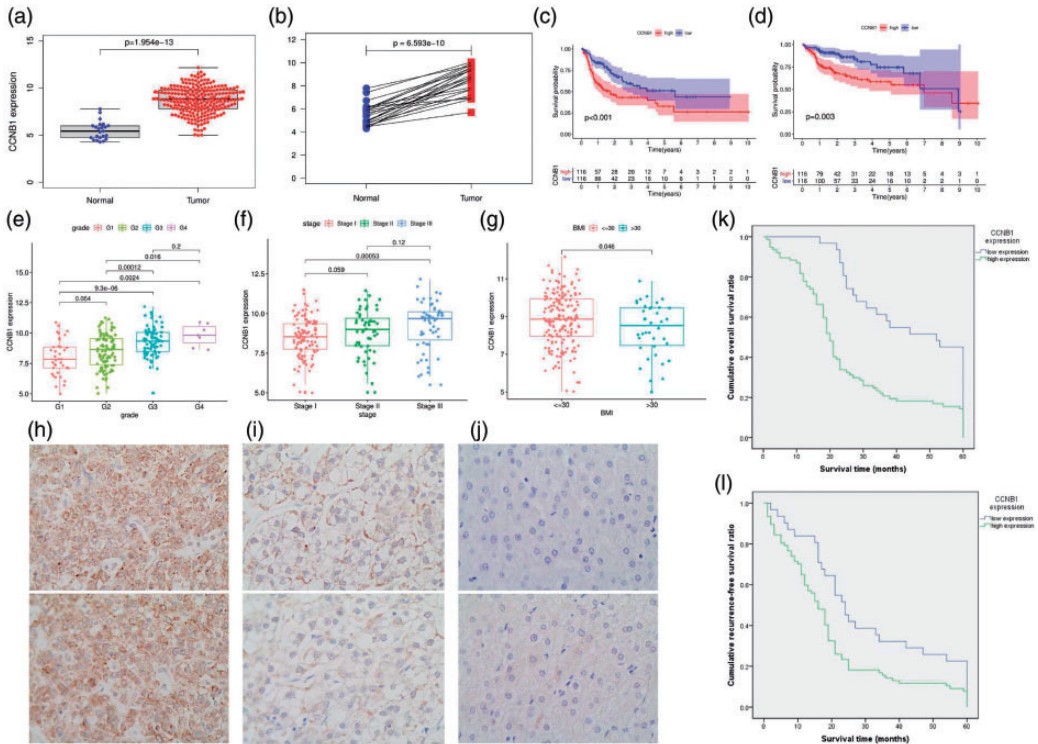


Figure 2. Cyclin B1 (CCNB1) is highly expressed in hepatocellular carcinoma (HCC) and suggests poor prognosis. (a) Differential expression of cyclin B1 (CCNB1) in normal liver and hepatocellular carcinoma (HCC) cases ($P < 0.001$). (b) Paired analysis of CCNB1 expression in normal and tumor samples of the same patients ($P < 0.001$). (c) Recurrence-free survival (RFS) ($P < 0.001$) and (d) overall survival (OS) analysis of the high vs. low CCNB1 expression groups ($P < 0.001$). (e) The relationship of CCNB1 expression and HCC grade. (f) The correlation of CCNB1 expression with tumor stage. (g) The correlation of CCNB1 expression with body mass index (BMI). (h) High expression of CCNB1 in HCC. (i) Low expression of CCNB1 in HCC. (j) Negative expression of CCNB1 in normal liver tissues. (k) OS and (l) RFS of HCC patients with high and low CCNB1 expression. The figures were produced by SPSS and R language with the packages of cluster Profiler and ggplot2.

(OS) of cases with high CCNB1 expression were significantly lower than those of the low expression cases (Figure 2c,d). In particular, the expression of CCNB1 was related to grade, stage, and BMI (Figures 2e–g). These results strongly suggested that CCNB1 expression was negatively correlated with HCC prognosis.

To further verify our observations, immunohistochemistry (IHC) assays were used to investigate the expression of CCNB1 in clinical HCC samples and liver tissues. As

shown in Figure 2h–j, CCNB1 expression was negative or extremely low in normal liver tissues, but upregulated in HCC slices. A correlation analysis exhibited the associations between CCNB1 expression and clinicopathological variables (Table 5), which demonstrated that high CCNB1 expression was associated with Hepatitis B surface antigen (HBsAg) ($P = 0.043$), MVI ($P = 0.047$), cirrhosis ($P = 0.037$), tumor differentiation ($P = 0.001$), and TNM stage ($P = 0.035$). Kaplan–Meier analysis showed that

Table 5. Association between cyclin B1 (CCNB1) protein expression and hepatocellular carcinoma (HCC) clinicopathological characteristics in 108 patients.

Variable	Number of Patients	CCNB1 protein level		P-value
		Low	High	
Age (years)	108			0.276
>50		27	60	
≤50		4	17	
Sex	108			0.166
Male		24	49	
Female		7	28	
HBsAg	108			0.043
Negative		17	26	
Positive		14	51	
Tumor size (cm)	108			0.487
≤5		26	60	
>5		5	17	
MVI	108			0.047
No		28	56	
Yes		3	21	
Cirrhosis	108			0.037
No		14	19	
Yes		17	58	
Tumor number	108			0.833
Single		18	43	
Multiple		13	34	
BMI	108			0.216
>23		8	12	
≤23		23	65	
Tumor differentiation	108			0.001
Moderate-Poor		5	38	
Well		26	39	
TNM stage	108			0.035
I/II		28	55	
III		3	22	

CCNB1, cyclin B1; HBsAg, Hepatitis B surface antigen; MVI, microvascular invasion; BMI, body mass index.

CCNB1 overexpression was associated with shorter OS ($P < 0.001$) and RFS ($P < 0.001$) (Figure 2k,l). The multivariate Cox regression analysis further indicated that high expression of CCNB1 could serve as an independent prognostic factor for OS (hazard ratio [HR] = 1.942, 95% confidence interval [CI] = 1.262–2.990, $P = 0.003$, Table 6) and RFS (HR = 1.609, 95% CI = 1.048–2.471, $P = 0.030$, Table 6).

CCNB1 knockdown inhibits the proliferation, invasion, and migration of HCC cells

A specific CCNB1 siRNA was transfected into HCC cell lines (Huh7 and HepG2), then CCNB1 protein expression levels were examined by immunofluorescence 72 hours after transfection (Figure 3a). Wound migration and Transwell

Table 6. Multivariate Cox regression analysis for various potential prognostic characteristics of overall survival (OS) and recurrence-free survival (RFS) in 108 hepatocellular carcinoma (HCC) patients.

Variable	Overall survival			Recurrence-free survival		
	Exp(B)	95% CI	P-value	Exp(B)	95% CI	P-value
Cirrhosis	1.412	0.906–2.202	0.128	1.160	0.739–1.819	0.519
Child–Pugh	1.566	0.793–3.091	0.196	1.954	0.998–3.824	0.051
Tumor differentiation	0.933	0.602–1.446	0.755	0.994	0.634–1.560	0.979
BMI	0.832	0.505–1.371	0.471	0.813	0.488–1.355	0.427
MVI	1.139	0.688–1.886	0.613	1.063	0.658–1.717	0.804
TNM stage	1.849	1.158–2.953	0.010	3.624	2.207–5.952	<0.001
CCNB1	1.942	1.262–2.990	0.003	1.609	1.048–2.471	0.030

CI, confidence interval; BMI, body mass index; MVI, microvascular invasion; CCNB1, cyclin B1.

experiments indicated that the migration ability of HCC cells with CCNB1 expression knocked down was significantly decreased (Figure 3b,d). CCK-8 experiments showed that CCNB1 siRNA transfection also significantly reduced the growth rates of Huh7 and HepG2 cells (Figure 3c). These data suggest that CCNB1 gene knockdown can inhibit the proliferation, invasion, and migration of HCC cells.

For *in vivo* experiments, the Huh7-sh CCNB1 and Huh7-shCtrl cells were subcutaneously inoculated into BALB/c nude mice. The average volume and weight of Huh7-sh CCNB1 tumors were markedly lower than those of Huh7-shCtrl tumors ($P < 0.01$) (Figure 3e). These results indicate that CCNB1 expression exerted a growth-promoting function in HCC.

CCNB1 is a potential biomarker of TME conversion

To further explore the potential role of CCNB1 in the HCC TME, GSEA was performed on the high and low CCNB1 expression groups. In the C7 gene set collection defined by MSigDB, the CCNB1 high expression group was enriched in multiple immunologic and immune functional gene

sets (Figure 4a). With GO, KEGG, and HALLMARK enrichment analyses, the gene sets in the high CCNB1 expression group were mainly enriched in cell cycle, DNA replication, and the P53 signaling pathway (Figure 4b–d). However, only one gene set was enriched in the low CCNB1 expression group (Figure 4e). The above results indicate that CCNB1 is a potential biomarker of TME conversion.

The relevance between CCNB1 and TIC proportions

A map of 22 immune cell types in HCC samples was constructed using the CIBERSORT computational method (Figure 4f,g). The correlation and difference analysis showed that there were nine types of TICs related to CCNB1 expression (Figure 5). Among them, CCNB1 was positively correlated with regulatory T cells (Tregs), follicular helper T cells, CD8+ T cells, CD4+ activated memory T cells, M0 macrophages, but negatively correlated with CD4+ naïve T cells, resting natural killer (NK) cells, resting mast cells, and M2 macrophages. These results further demonstrate that CCNB1 levels can influence the immune activity of the HCC TME.

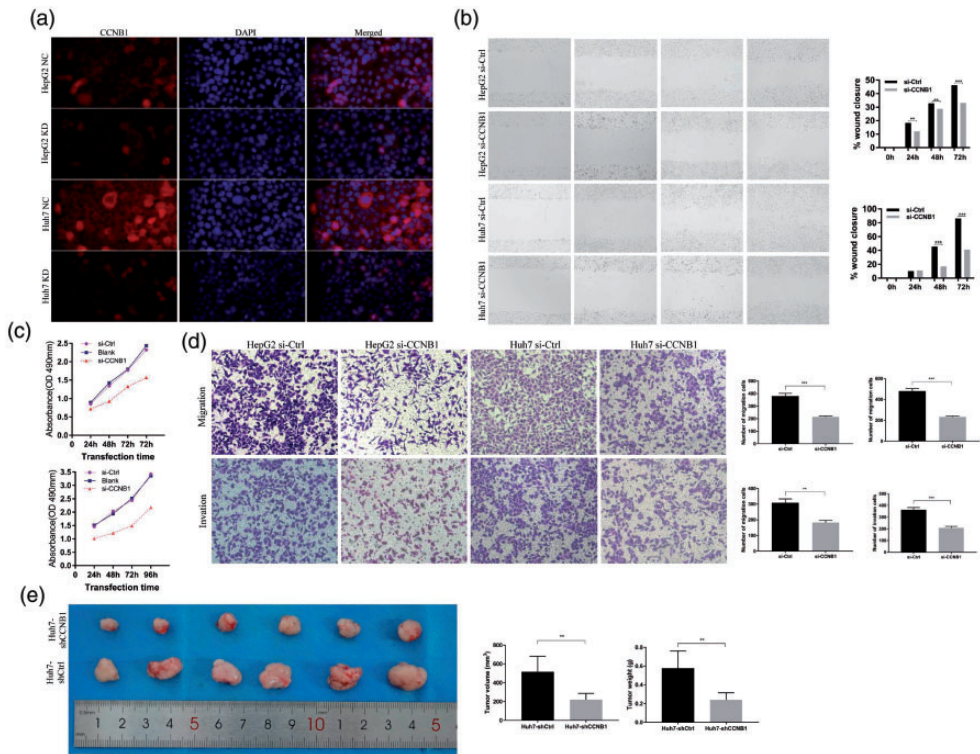


Figure 3. Cyclin BI (CCNB1) knockdown inhibits the proliferation, invasion, and migration of hepatocellular carcinoma (HCC) cells *in vitro* and *in vivo*. (a) The transfection efficiency of small interfering RNAs (siRNAs) in HepG2 and Huh7 cells. (b) Wound-healing assays indicate that silencing of cyclin BI (CCNB1) can inhibit HepG2 and Huh7 cell migration. (c) Cell proliferation was determined by Cell Counting Kit (CCK)-8 assays and detected at 24, 48, 72, and 96 hours after siRNA transfection. (d) Transwell experiments demonstrate that knockdown of CCNB1 can significantly reduce the migratory and invasive abilities of hepatocellular carcinoma (HCC) cells. (e) The Huh7-shCCNB1 and Huh7-shCtrl cells were subcutaneously inoculated into the left-side axilla of BALB/c nude mice (n = 6/group). Data points are presented as the mean ± standard deviation (SD) for tumor volume and weight. The graph was generated using GraphPad Prism.

Discussion

HCC is a common and lethal malignancy that is often diagnosed at an advanced stage. High genetic heterogeneity was once considered the main cause of treatment failure.¹⁹ However, accumulating evidence has shown that HCC invasion and metastasis are the results of the co-evolution of cancer cells and microenvironment.²⁰

In solid tumors, the cancer cells are wrapped in an intricate mixture of

nontumorous cells and matrix components that are denominated as the TME. The TME is essential for tumor formation and progression, including angiogenesis and metastasis. Moreover, it has been shown to influence the effectiveness of anti-tumor therapies. Hence, lubricating the tumor stroma would improve the curative effect of current treatment methods and provide new opportunities for therapeutic targeting.^{21,22} Recent work has suggested that

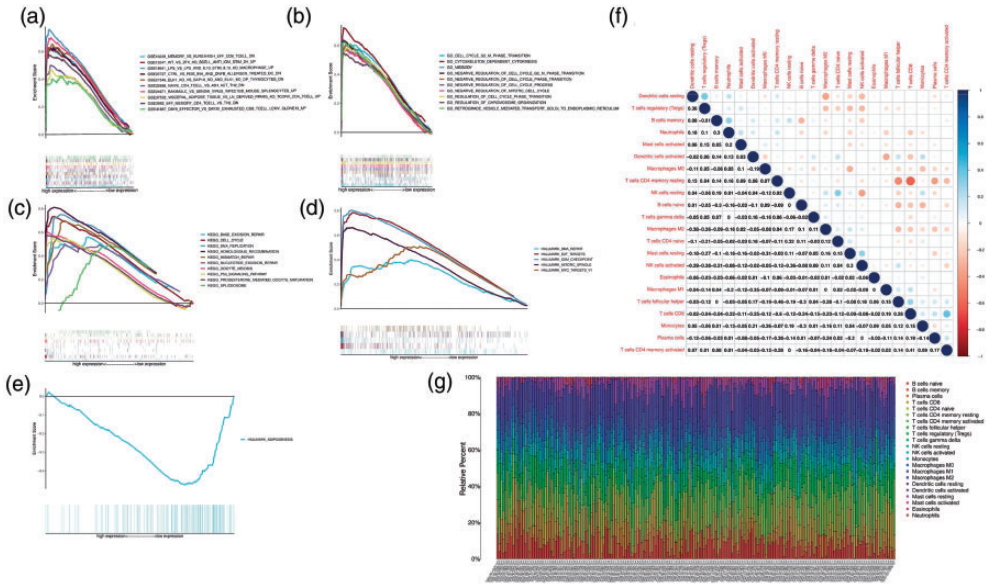


Figure 4. Gene Set Enrichment Analysis (GSEA) for cases with high cyclin B1 (CCNB1) expression and the proportion and correlation analysis of tumor-infiltrating immune cells (TICs) in hepatocellular carcinoma (HCC) cases. (a) C7 collection enriched gene sets in the cyclin B1 (CCNB1) overexpression group (Gene sets with nominal (NOM) $P < 0.05$ and FDR $q < 0.05$ were considered to be significant. The top 10 gene sets are shown in the map). (b) Gene Ontology (GO) collection-enriched gene sets in the CCNB1 overexpression group. (c) Kyoto Encyclopedia of Genes and Genomes (KEGG) collection-enriched gene sets in the CCNB1 overexpression group. (d) HALLMARK collection-enriched gene sets in the CCNB1 overexpression group. (e) The HALLMARK collection-enriched gene set in the low CCNB1 expression group. (f) The interrelationship among 22 types of tumor-infiltrating immune cells (TICs) (Pearson coefficient test). Each number represents the correlation P -value between every two types of immune cells. The color depth indicates the corresponding correlation value between two types of cells. (g) The proportion of 22 TICs in HCC cases. The figures were generated using Gene Set Enrichment Analysis (GSEA) and R language.

boosting the number of neutrophils induced by administering granulocyte colony stimulating factor (G-CSF) would lead to increased tumor aggressiveness.²³ In coculture experiments, macrophages reduced the sensitivity of cancer cells to doxorubicin, etoposide, paclitaxel, and cisplatin, which was achieved by producing signal transducer and activator of transcription 3 (STAT3), inflammatory modulators,²⁴ cathepsin B,²⁵ and exosomes,²⁶ respectively. During chemotherapy, DNA damage in stromal cells, especially endothelial cells, increases the activity of NF- κ B and numerous cytokines that protect tumor cells from DNA damage.²⁷ In addition, fibroblasts and

extracellular matrix increase the tumor interstitial pressure, thus reducing the effect of the chemotherapeutic agent.²⁸ During radiotherapy, fibroblasts are activated to synthesize a mass of collagens and arrange into dense fibrous tissue, which promotes cancer cell survival through the integrin signaling pathway.²⁹ Similar to cytotoxic drugs, radiation-induced DNA damage leads to fibroblast senescence and promotes the synthesis of a secretome containing high levels of transforming growth factor (TGF)- β , vascular endothelial growth factor (VEGF)-A, and various cytokines.³⁰ Furthermore, the immunosuppressive effects of TGF- β

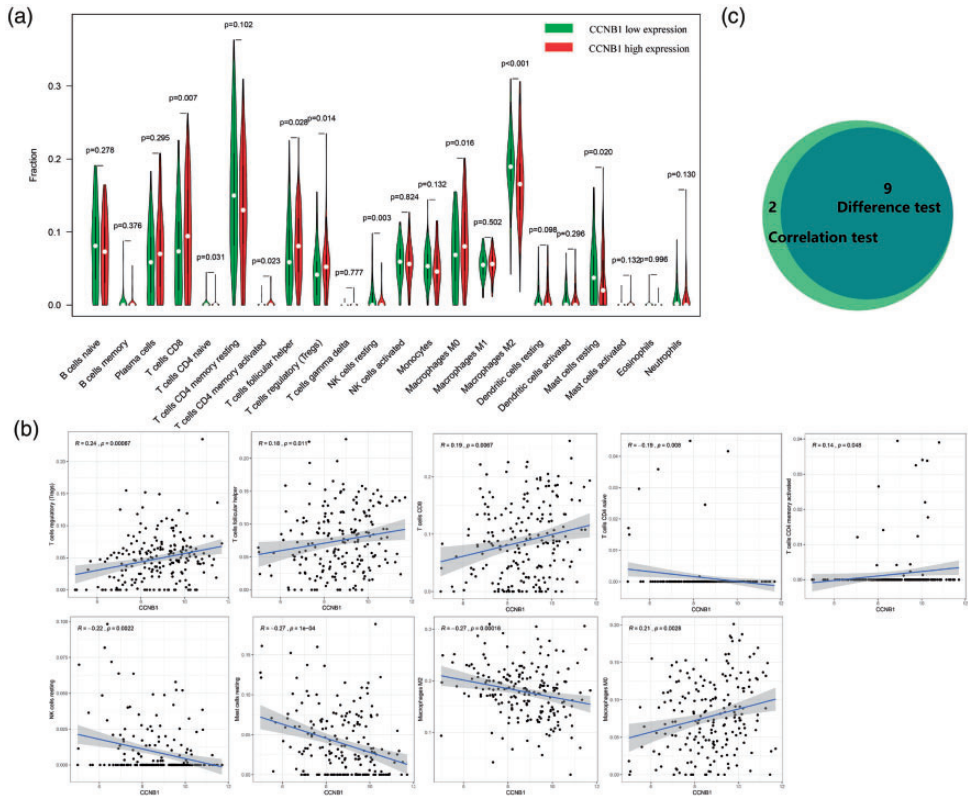


Figure 5. Relationship between tumor-infiltrating immune cell (TIC) proportions and cyclin B1 (CCNB1) expression. (a) The proportion differences of 22 types of immune cells in the high vs. low cyclin B1 (CCNB1) expression groups. (b) Tumor-infiltrating immune cells (TICs) related to CCNB1 expression ($P < 0.05$). (c) TICs correlated with CCNB1 expression codetermined by difference and correlation tests. The figures were generated using R language with the CIBERSORT calculation method.

reduces the CD8-mediated killing effect on tumor cells.³¹ Thus, the TME has been shown to modulate the response to anti-tumor therapies. Additionally, lucubrating the TME may improve the efficacy of current therapies and provide new opportunities for therapeutic targeting.

In this study, we provide data suggesting that the immune and stromal scores calculated by the ESTIMATE algorithm are correlated with clinicopathological factors in HCC. Lower stromal and immune scores are associated with worse prognosis. Based on this theoretical basis, we then extracted 546 genes involved in the TME,

127 of which were associated with RFS. In addition, we verified 103 genes in HCC cohort GSE54236. Using PPI networks, we confirmed that CCNB1 could be used as an independent prognostic factor for HCC.

CCNB1 is a key modulator of cell cycle regulation and has been shown to be over-expressed in several human cancers.³² Song et al. demonstrated that CCNB1 promotes tumor invasion and metastasis by enhancing epithelial-mesenchymal transition (EMT).³³ Lu et al. confirmed that inhibiting CCNB1/CDK1 restores p53 function, suggesting that CCNB1 could promote

tumorigenesis by impairing p53 function.³⁴ In addition, Ding et al. demonstrated that CCNB1 enhanced drug resistance in breast cancer hormone therapy.³⁵ High levels of CCNB1 indicated that the treatment would be ineffective, including tamoxifen and aromatase inhibitors.³⁶ Here, we began with analysis of HCC transcriptome data from TCGA database and clinical patients. We then confirmed that CCNB1 was significantly overexpressed in HCC tissues, and this up-regulation was associated with advanced clinicopathological features (including HBsAg, MVI, cirrhosis, tumor differentiation, and TNM stage) and poor prognosis. CCNB1 knockdown inhibited the proliferation, invasion, and migration of HCC cells both *in vitro* and *in vivo*. Therefore, CCNB1 has the potential to be a prognostic biomarker and therapeutic target for the HCC TME.

After further exploration of the correlation between CCNB1 expression and the TME, GSEA results revealed that, in addition to cell cycle-related signaling pathways, immune cell-related signaling pathways were also significantly enriched in the CCNB1 high-expression group, especially for T lymphocytes. However, only the adipogenesis pathway was enriched in the CCNB1 low-expression group. The above-mentioned results suggest that CCNB1 may participate in the regulation of immune cell function and the status conversion of fat metabolism. Subsequence analysis on TICs corroborated this viewpoint. Our CIBERSORT analysis of TIC proportions showed that, along with the upregulation of CCNB1, M0 macrophages could undergo differentiation inhibition. Additionally, T cells showed abnormal activation with altered functions. These results supported that CCNB1 could promote HCC. However, a limitation of this study is the lack of further discussion regarding the regulatory role of CCNB1. Thus, the

functional mechanisms of CCNB1 still require further experimental verification.

Conclusion

The interaction between HCC and the TME greatly affects tumor progression, therapeutic effects, and prognosis. In this work, we focused on the impact of microenvironment-related genes on RFS in HCC patients. Our results provide more data to unravel the complex interactions between HCC tumor cells and the TME. In summary, using the ESTIMATE algorithm-based scores, a gene list related to the TME was extracted. Some previously overlooked genes have the potential to become new tumor markers or therapeutic targets. CCNB1 is a potential prognostic factor and cancer promoter in HCC cases. In addition, CCNB1 may serve as a hub gene that regulates other DEGs, and could possibly be used as an indicator of TME state transition. Hence, further research should be conducted to clarify the relationship between CCNB1 expression and immune cell function.

Acknowledgment

We appreciate Dr. Yingjuan Xu's help with this manuscript, as well as with guidance on data collection and processing.

Declaration of conflicting interest

The authors declare that there is no conflict of interest.

Funding

This research received no specific grant from any funding agency in the public, commercial, or not-for-profit sectors.

ORCID iDs

Xinbo Liu  <https://orcid.org/0000-0001-7576-0061>

Dequan Wu  <https://orcid.org/0000-0002-1232-6409>

References

1. Bray F, Ferlay J, Soerjomataram I, et al. Global cancer statistics 2018: GLOBOCAN estimates of incidence and mortality worldwide for 36 cancers in 185 countries. *CA Cancer J Clin* 2018; 68: 394–424. doi:10.3322/caac.21492
2. Simard EP, Ward EM, Siegel R, et al. Cancers with increasing incidence trends in the United States: 1999 through 2008. *CA Cancer J Clin* 2012; 62: 118–128. doi:10.3322/caac.20141
3. Weinstein JN, Collisson EA, Mills GB, et al. The cancer genome atlas pan-cancer analysis project. *Nat Genet* 2013; doi:10.1038/ng.2764
4. Yoshihara K, Shahmoradgoli M, Martínez E, et al. Inferring tumour purity and stromal and immune cell admixture from expression data. *Nat Commun* 2013; 4: 2612. doi:10.1038/ncomms3612
5. Hanahan D and Coussens LM. Accessories to the Crime: Functions of Cells Recruited to the Tumor Microenvironment. *Cancer Cell* 2012; 21: 309–322. doi:10.1016/j.ccr.2012.02.022
6. Ye L, Li Y, Tang H, et al. CD8+CXCR5+T cells infiltrating hepatocellular carcinomas are activated and predictive of a better prognosis. *Aging (Albany NY)* 2019; 11: 8879–8891. doi:10.18632/aging.102308
7. Shah N, Wang P, Wongvipat J, et al. Regulation of the glucocorticoid receptor via a BET-dependent enhancer drives antiandrogen resistance in prostate cancer. *Elife* 2017; 6: e27861. doi:10.7554/eLife.27861
8. Priedigkeit N, Watters RJ, Lucas PC, et al. Exome-capture RNA sequencing of decade-old breast cancers and matched decalcified bone metastases. *JCI Insight* 2017; 2: e95703. doi:10.1172/jci.insight.95703
9. Alonso MH, Aussó S, Lopez-Doriga A, et al. Comprehensive analysis of copy number aberrations in microsatellite stable colon cancer in view of stromal component. *Br J Cancer* 2017; 117: 421–431. doi:10.1038/bjc.2017.208
10. Jia D, Li S, Li D, et al. Mining TCGA database for genes of prognostic value in glioblastoma microenvironment. *Aging (Albany NY)* 2018; 10: 592–605. doi:10.18632/aging/101415
11. Miyazaki T and Arai S. Two distinct controls of mitotic cdk1/cyclin B1 activity requisite for cell growth prior to cell division. *Cell Cycle* 2007; 6: 1419–1425.
12. Takizawa CG and Morgan DO. Control of mitosis by changes in the subcellular location of cyclin-B1-Cdk1 and Cdc25C. *Curr Opin Cell Biol* 2000; 12: 658–665. doi:10.1016/S0955-0674(00)00149-6
13. Ritchie ME, Phipson B, Wu D, et al. Limma powers differential expression analyses for RNA-sequencing and microarray studies. *Nucleic Acids Res* 2015; 43: e47. doi:10.1093/nar/gkv007
14. Metsalu T and Vilo J. ClustVis: A web tool for visualizing clustering of multivariate data using Principal Component Analysis and heatmap. *Nucleic Acids Res* 2015; 43: W566–W570. doi:10.1093/nar/gkv468
15. Szklarczyk D, Franceschini A, Wyder S, et al. STRING v10: Protein-protein interaction networks, integrated over the tree of life. *Nucleic Acids Res* 2015; 43(Database issue): D447–D452. doi:10.1093/nar/gku1003
16. Shannon P, Markiel A, Ozier O, et al. Cytoscape: A software Environment for integrated models of biomolecular interaction networks. *Genome Res* 2003; 13: 2498–2504. doi:10.1101/gr.1239303
17. Bandettini WP, Kellman P, Mancini C, et al. MultiContrast Delayed Enhancement (MCOE) improves detection of subendocardial myocardial infarction by late gadolinium enhancement cardiovascular magnetic resonance: A clinical validation study. *J Cardiovasc Magn Reson* 2012; 14: 83. doi:10.1186/1532-429X-14-83
18. Villa E, Critelli R, Lei B, et al. Neoangiogenesis-related genes are hallmarks of fast-growing hepatocellular carcinomas and worst survival. results from a prospective study. *Gut* 2016; 65: 861–869. doi:10.1136/gutjnl-2014-308483
19. Gao Q, Wang ZC, Duan M, et al. Cell Culture System for Analysis of Genetic Heterogeneity Within Hepatocellular Carcinomas and Response to

- Pharmacologic Agents. *Gastroenterology* 2017; 152: 232–242.e4. doi:10.1053/j.gastro.2016.09.008
20. Kurebayashi Y, Ojima H, Tsujikawa H, et al. Landscape of immune microenvironment in hepatocellular carcinoma and its additional impact on histological and molecular classification. *Hepatology* 2018; 68: 1025–1041. doi:10.1002/hep.29904
 21. Wood SL, Pernemalm M, Crosbie PA, et al. The role of the tumor-microenvironment in lung cancer-metastasis and its relationship to potential therapeutic targets. *Cancer Treat Rev* 2014; 40: 558–566. doi:10.1016/j.ctrv.2013.10.001
 22. Quail DF and Joyce JA. Microenvironmental regulation of tumor progression and metastasis. *Nat Med* 2013; 19: 1423–1437. doi:10.1038/nm.3394
 23. Antonio N, Bønnelykke-Behrndtz ML, Ward LC, et al. The wound inflammatory response exacerbates growth of pre-neoplastic cells and progression to cancer. *EMBO J* 2015; 34: 2219–2236. doi:10.15252/embj.201490147
 24. Mitchem JB, Brennan DJ, Knolhoff BL, et al. Targeting tumor-infiltrating macrophages decreases tumor-initiating cells, relieves immunosuppression, and improves chemotherapeutic responses. *Cancer Res* 2013; 73: 1128–1141. doi:10.1158/0008-5472.CAN-12-2731
 25. Bruchard M, Mignot G, Derangère V, et al. Chemotherapy-triggered cathepsin B release in myeloid-derived suppressor cells activates the Nlrp3 inflammasome and promotes tumor growth. *Nat Med* 2013; 19: 57–64. doi:10.1038/nm.2999
 26. Challagundla KB, Wise PM, Neviani P, et al. Exosome-Mediated Transfer of microRNAs Within the Tumor Microenvironment and Neuroblastoma Resistance to Chemotherapy. *J Natl Cancer Inst* 2015; 107: djv135. doi:10.1093/jnci/djv135
 27. Tavora B, Reynolds LE, Batista S, et al. Endothelial-cell FAK targeting sensitizes tumours to DNA-damaging therapy. *Nature* 2015; 514: 112–116. doi:10.1038/nature13541
 28. Olive KP, Jacobetz MA, Davidson CJ, et al. Inhibition of Hedgehog signaling enhances delivery of chemotherapy in a mouse model of pancreatic cancer. *Science* 2009; 324: 1457–1461. doi:10.1126/science.1171362
 29. Shu CL, Jing-Yang-Lai, Su LC, et al. SWAP-70: A New Type of Oncogene. *PLoS One* 2013; 8: e59245. doi:10.1371/journal.pone.0059245
 30. Freund A, Orjalo AV, Desprez PY, et al. Inflammatory networks during cellular senescence: causes and consequences. *Trends Mol Med* 2010; 16: 238–246. doi:10.1016/j.molmed.2010.03.003
 31. Vanpouille-Box C, Diamond JM, Pilonis KA, et al. TGF β is a master regulator of radiation therapy-induced antitumor immunity. *Cancer Res* 2015; 75: 2232–2242. doi:10.1158/0008-5472.CAN-14-3511
 32. Huang V, Place RF, Portnoy V, et al. Upregulation of Cyclin B1 by miRNA and its implications in cancer. *Nucleic Acids Res* 2012; 40 :1695–707. doi:10.1093/nar/gkr934
 33. Song Y, Zhao C, Dong L, et al. Overexpression of cyclin B1 in human esophageal squamous cell carcinoma cells induces tumor cell invasive growth and metastasis. *Carcinogenesis* 2008; 29: 307–315. doi:10.1093/carcin/bgm269
 34. Lu M, Breysens H, Salter V, et al. Restoring p53 Function in Human Melanoma Cells by Inhibiting MDM2 and Cyclin B1/CDK1-Phosphorylated Nuclear iASPP. *Cancer Cell* 2013; 23: 618–633. doi:10.1016/j.ccr.2013.03.013
 35. Ding K, Li W, Zou Z, et al. CCNB1 is a prognostic biomarker for ER+ breast cancer. *Med Hypotheses* 2014; 83: 359–364. doi:10.1016/j.mehy.2014.06.013
 36. Miller WR. Clinical, pathological, proliferative and molecular responses associated with neoadjuvant aromatase inhibitor treatment in breast cancer. In: *Journal of Steroid Biochemistry and Molecular Biology* 2010; 118: 273–276. doi:10.1016/j.jsbmb.2009.10.005

Appendix

Differentially expressed genes (DEGs) significantly associated with poor recurrence-free survival (RFS)

C12orf48	CENPF	C21orf58	IQCH	E2F1	TRAIP	LOC100133612	CXorf57
UBE2C	EXO1	ESM1	RNASEH2A	CDCA2	CDCA3	FAM72D	RNF157
TPX2	EME1	PRIM1	LOC388152	NUF2	ASPM	KIF4A	LOC100128191
TRIP13	KIF15	LOC80154	CDKN3	CHEK1	FOXM1	ZNRF3	ORC1L
ZWINT	C15orf42	DHRS13	CELSR3	SKA3	CDC25A	SNHG7	CPLX2
PSMC3IP	KIFC1	HMMR	STL	NFKBIL2	SKA1	AURKB	C7orf29
TTK	PTTGI	C6orf26	SPC24	CDK1	DEPDC1	FAM57B	TERT
TOP2A	UBE2T	GAS5	CGREF1	CECR4	C9orf100	CCNB1	LOC339674
NEIL3	HOXD10	FAM83D	TPTE	POLQ	CDT1	BIRC5	SGOL1
NT5C3L	RECQL4	CCNB2	POC1A	TROAP	CDC6	CENPM	E2F7
ERCC6L	OIP5	LRRC45	PRDM12	NDC80	SAC3D1	MELK	CDC20
CDCA5	KIF18B	MXD3	HTR1D	CENPA	CDC25C	KIF18A	HOXD9
RAD54L	DTL	EPR1	EIF3C	BUB1B	ASF1B	KIF2C	SPC25
KIAA0101	C12orf39	NCAPG	FATE1	C16orf59	THBS4	RDM1	CHGA
C17orf53	FBXO43	GINS1	CDKN2BAS	FAM161A	SNHG3	TK1	PPFIA4
HJURP	DIAPH3	KIF20A	MYBL2	NEK2	FAM72B	RAC3	